Published in final edited form as:
Small. 2014 February 12; 10(3): 544–555. doi:10.1002/smll.201301593.

Active Targeting Using HER-2-affibody-conjugated Nanoparticles Enabled Sensitive and Specific Imaging of Orthotopic HER-2 Positive Ovarian Tumors

Dr. Minati Satpathy,
Emory University School of Medicine, Atlanta, GA

Dr. Liya Wang,
Emory University School of Medicine, Atlanta, GA

Rafal Zielinski,
MD. Anderson Cancer Center, Houston, TX

Dr. Weiping Qian,
Emory University School of Medicine, Atlanta, GA

Dr. Malgorzata Lipowska,
Emory University School of Medicine, Atlanta, GA

Dr. Jacek Capala,
Radiation Oncology, National Institutes of Health, Bethesda, MD

Dr. Gee Young Lee,
Emory University School of Medicine, Atlanta, GA

Dr. Hong Xu,
Ocean Nanotech, LLC, Springdale, AR

Dr. Y. Andrew Wang,
Ocean Nanotech, LLC, Springdale, AR

Dr. Hui Mao, and
Emory University School of Medicine, Atlanta, GA.

Dr. Lily Yang*
Emory University School of Medicine, Atlanta, GA

Abstract

Despite advances in cancer diagnosis and treatment, ovarian cancer remains one of the most fatal cancer types. The development of targeted nanoparticle imaging probes and therapeutics offers promising approaches for early detection and effective treatment of ovarian cancer. In this study, we have developed HER-2 targeted magnetic iron oxide nanoparticles (IONPs) by conjugating a high affinity and small size HER-2 affibody that is labeled with a unique near infrared dye

*Prof. Lily Yang, Department of Surgery, Emory University School of Medicine, Clinic C, Room C-4088, 1365 C Clifton Road, NE, Atlanta, GA 30322. Telephone: 404-778-4269; Fax: 404-778-5530. Lyang02@emory.edu.

(NIR-830) to the nanoparticles. Using a clinically relevant orthotopic human ovarian tumor xenograft model, we have shown that HER-2 targeted IONPs are selectively delivered into both primary and disseminated ovarian tumors, enabling non-invasive optical and MR imaging of the tumors as small as 1 mm in the peritoneal cavity. We have determined that HER-2 targeted delivery of the IONPs is essential for specific and sensitive imaging of the HER-2 positive tumor since we are unable to detect the imaging signal in the tumors following systemic delivery of non-targeted IONPs into the mice bearing HER-2 positive SKOV3 tumors. Furthermore, imaging signals and the IONPs are not detected in HER-2 low expressing OVCAR3 tumors after systemic delivery of HER-2 targeted-IONPs. Since HER-2 is expressed in a high percentage of ovarian cancers, the HER-2 targeted dual imaging modality IONPs have potential for the development of novel targeted imaging and therapeutic nanoparticles for ovarian cancer detection, targeted drug delivery, and image-guided therapy and surgery.

Keywords

HER-2 targeted nanoparticles; HER-2 affibody; NIR-830 dye; orthotopic human ovarian tumor xenograft model

1. Introduction

Ovarian cancer is the fifth leading cause of cancer death among women. The disease is typically asymptomatic till advanced stages.[1–3] Absence of an anatomical barrier promotes early spread of the cancer cells to the peritoneal cavity.[4] Currently surgical staging and resection followed by chemotherapy are the standard regimen for ovarian cancer.[5] However these therapeutic approaches are not very effective for advanced ovarian cancer and the five-year survival rate of the patients is only 30%.[6] Therefore, there is an urgent need to develop novel approaches for early detection and effective treatment of ovarian cancer.

The major problems in the clinical management of ovarian cancer are early detection, accurately staging, sensitive detection of disseminated tumors in the peritoneal cavity, and chemoresistance.[7] Targeted imaging probes for non-invasive imaging have potential to enhance specificity and sensitivity of cancer detection as well as assist in accurate tumor staging for selection of treatment strategies. Combination of novel intraoperative imaging devices with targeted imaging probes should allow image-guided surgery for complete removal of cancer lesions during the debulking surgery. Currently, gadolinium contrast enhanced magnetic resonance imaging (MRI) and computed tomography (CT) are used for the detection and staging of ovarian cancer.[6] However, they lack desirable specificity and sensitivity for non-invasive tumor imaging and are not adequate for image-guided surgery. PET/CT has been used for preoperative cancer imaging but it is not suitable for intraoperative imaging due to the use of radioactive tracers and a low spatial resolution to determine the location of ovarian tumors.[8]

The human epidermal growth factor receptor 2 (HER-2/*neu*) is overexpressed in many tumor types including ovarian cancer.[9–17] HER-2 has been considered as an important biomarker for the development of tumor targeted imaging and therapy agents.[18] HER-2

targeted nanoparticles were produced using monoclonal antibodies against HER-2/*neu* and their effects on tumor imaging and targeted therapy have been shown in various animal tumor models.[19, 20] Recently, a HER-2 specific affibody that is based on a 58-amino-acid protein scaffold with the binding affinity at a picomolar range has been developed as a targeting ligand for the production of optical and positron emission tomography (PET)/imaging probes.[21–24] Radiolabeled HER-2 affibody has been used as a PET imaging probe in clinical trials for determination of the level of HER-2 expression and for monitoring response to HER-2-targeted therapy in breast cancer patients.[25] This small size high affinity ligand is an excellent candidate for engineering compact size HER-2 targeted nanoparticles with the ability of multivalent and high affinity binding to HER-2 receptors and promoting efficient internalization of the nanoparticle-receptor complexes. HER-2 affibody has been conjugated to nanoparticles such as quantum dots (QDs), iron oxide nanoparticles (IONPs), and polymeric nanoparticles.[26–28] HER-2 affibody-QDs have been shown to be able to selectively accumulate in subcutaneous human ovarian cancer xenografts in nude mice and were detectable by optical imaging.[26] However, in subcutaneous ovarian tumor models, it is unclear whether the HER-2 affibody-nanoparticle is able to target both primary and metastatic cancer lesions for sensitive tumor imaging and efficient delivery of therapeutics. For clinical translations of HER-2 targeted tumor imaging and therapy approaches, this is an important issue to be considered in designing a targeted nanoparticle as well as in conducting preclinical studies in animal tumor models.

IONPs have been used in human patients as non-targeted MR contrast agents for the detection of liver cancer or lymph node metastases.[29, 30] However, such an approach relied on the enrichment of the nanoparticles in normal tissues that created a contrast in the tumor, which lacked sensitivity and specificity. IONPs with dual optical and MR imaging modalities have been developed by labeling fluorescence dye molecules to IONPs.[31–34] Cross linked iron oxide (CLIO) nanoparticles with a dextran coating were the first dual imaging probes that were conjugated with tumor targeting ligands, enabling tumor specific optical and MR imaging in several animal tumor models.[35–37] Several other targeted dual imaging IONP probes with various polymer surface coating have also been developed for tumor imaging.[38–40] However, most previous studies, including ours, used Cy5.5 NIR dye either directly labeled onto the IONPs,[32, 34] or on targeting ligands that were conjugated to the IONPs.[33] Cy5.5 dye has a maximal emission wavelength of 697 nm, which overlaps with body background fluorescence emitted by hemoglobin, and therefore, has a relatively low sensitivity in tumor imaging.[31] To increase specificity and sensitivity of tumor imaging, we developed optical and MR dual imaging HER-2 targeted magnetic IONPs by conjugating HER-2 affibody ($Z_{HER2:342}$) targeting ligands that were labeled with a unique near infrared (NIR-830) dye to amphiphilic polymer-coated IONPs. A major advantage of this nanoparticle is that NIR-830 dye-labeled targeting ligand with excitation/emission wavelengths of 800/825 nm, developed by our group, enables optical imaging of the tumor with high tumor signal and low background noise, while magnetic IONPs provide strong MRI contrasts as well as efficient drug carriers.[41] In this study, we demonstrated the ability of systemic delivery of NIR-830-$Z_{HER2:342}$-IONPs in targeting primary and metastatic tumors in an orthotopic human ovarian cancer xenograft model using NIR optical and T_2-weighted MR imaging, and histological analysis of the tumor tissues and normal organs. Our

results support further development of this HER-2 targeted IONP as dual imaging modality probes and theranostic nanoparticles.

2. Results

2.1 Characterization of NIR-830-$Z_{HER2:342}$-IONPs

To determine the sensitivity and specificity of HER-2 targeted IONPs in tumor targeting using optical and MR imaging, we produced two types of IONP conjugates. HER-2-targeted IONPs were generated by conjugating ten HER-2 affibody molecules ($Z_{HER2:342}$-Cys) that were pre-labeled with one NIR-830 dye per HER-2 affibody to one polymer-coated IONP (NIR-830-$Z_{HER2:342}$-IONP) as described in Experimental Section (Figure 1A and Supporting Information S1). Control non-targeted IONPs were produced by conjugating ten NIR-830 dye labeled bovine serum albumin (BSA) onto one IONP (NIR-830-BSA-IONP). The IONP conjugates were fully characterized for their particle size, stability, and binding specificity. Dynamic light scattering (DLS) measurement showed that the hydrodynamic diameters of non-conjugated IONP, NIR-830-$Z_{HER2:342}$-IONPs, and non-targeted NIR-830-BSA-IONPs were 14 ± 3.4 nm, 18.2 ± 2.6 nm, and 22.9 ± 4.8 nm, respectively (Figure 1B). Targeted IONPs were stable at 4ºC for more than 6 months in pH 8.6 Borate buffer and retained the same hydrodynamic size. The Zeta potential value for non-conjugated IONPs was −30.3 ± 2.99 mv. After conjugating with $Z_{HER2:342}$ and BSA, the values of zeta potentials increased to −30.9 ± 0.69 mv and −32.4 ± 1.15 mv respectively. Spectroscopic measurement of the NIR-830-$Z_{HER2:342}$-IONPs showed that the NIR signal peaked at an emission wavelength of 825 to 830 nm (Figure 1C). Results of Western blot and immunofluorescence analyses showed a markedly higher level of HER-2 expression in SKOV3 human ovarian cancer cells compared to OVCAR3 cells (Figure 1D and E). Incubation of NIR-830-$Z_{HER2:342}$-IONPs with above cells led to the binding and internalization of the nanoparticles in SKOV3 but not in OVCAR3 cells, which was validated by Prussian blue staining (Figure 1F). However, incubation of both cell lines with non-targeted IONPs showed very low levels of Prussian blue staining (Figure 1F).

2.2 Targeted delivery of NIR-830-$Z_{HER2:342}$-IONPs into primary and metastatic tumors

Sensitive and specific detection of ovarian cancers is one of the major challenges in the clinic because of the location of the primary tumor deep in the pelvis and dissemination of tumor lesions spreading in the peritoneal cavity. We established orthotopic ovarian tumor xenograft models in nude mice (Supporting Information, S2) to precisely evaluate the efficiency of targeted nanoparticle delivery into primary and metastatic tumors. To determine if non-invasive NIR optical imaging has sufficient sensitivity to detect small ovarian tumors in the peritoneal cavity, tumor-bearing mice at 1 and 2 weeks following the cell implantation were injected with NIR-830-$Z_{HER2:342}$-IONPs. We found that the early stage tumors with diameters of 1 to 2 mm were detectable by non-invasive NIR optical imaging. We detected a tumor signal to body background (S/B) ratio of 1.6 ± 0.09 (n=5, 1 week tumor) or 1.9 ± 0.37 (n=3, 2 week tumor) folds, suggesting that the selective accumulation of the NIR-830-$Z_{HER2:342}$-IONPs in the tumor allowed sensitive imaging of small ovarian tumors (Figure 2A). *Ex vivo* optical imaging of the tumor and normal organs confirmed the presence of a high level of the optical signals in the tumor. In normal organs,

the signal was found in the kidney and liver but not in any other organs (Figure 2B). We also noticed that signal intensities of the liver and kidney detected in *ex vivo* imaging were usually higher than that of non-invasive imaging. The presence of the IONP positive cells in the tumor tissues was further verified by Prussian blue staining of tissue sections (Figure 2C). As expected, the liver and spleen showed non-specific iron uptake, most likely by Kupffer cells or macrophages (Figure 2C). Although strong optical signal was seen in the kidney, iron staining was negative in the kidney tissue section. This may be due to the renal clearance of free dye molecules or break down products of targeting ligands, and the lack of non-specific macrophage uptake of the IONPs in the kidney to retain the nanoparticles in the tissue sections. However, optical signals produced by small tumors in non-invasive imaging at 24 h following the nanoparticle injection were still 1.2 to 1.6 folds higher than that of the kidney (Figure 2A).

Next, we investigated target specificity in the advanced stage tumors by injecting NIR-830-$Z_{HER2:342}$-IONPs in the tumor bearing mice at 6 weeks or above after cell implantation, which have both primary SKOV3 tumors over 6 mm in diameter and metastatic lesions. Non-invasive NIR optical imaging showed the strongest signal in the primary tumor with an T/B ratio of 2.9 ± 1.19 (n=9) and 2.06 ± 0.75 fold higher signal over the kidney (n=3) (Figure 3A). Additionally, small metastatic lesions in the peritoneal cavity were detected in optical images obtained from both dorsal and ventral sides (Figure 3A). All five tumor lesions shown on BLI could also be identified by non-invasive NIR imaging (Figure 3A). Small metastatic tumors in the peritoneal cavity showed 2.1 to 2.5-fold higher signal compared with body background signal. *Ex vivo* organ imaging showed bright NIR signals in the large primary tumor, a small metastatic tumor (~1 mm), the kidney, and the liver (Figure 3A). Prussian blue staining revealed the presence of IONP positive cells in both peripheral and central tumor areas (Figure 3A). High magnification microscopic image demonstrated internalization of the IONPs into the tumor cells (Figure 3A). IONP positive cells were observed in the liver and spleen but not in the heart and kidney (Figure 3A).

Although pulmonary metastasis is a rare event in human ovarian cancer patients [42], we were able to detect the lung metastasis in the tumor bearing mice by BLI as well as NIR optical imaging after injecting NIR-830-$Z_{HER2:342}$–IONPs (Figure 3B). *Ex vivo* imaging and histological analysis by H&E or Prussian blue staining further demonstrated the presence of the iron positive tumor cells in the lung (Figure 3B). Thus, our results support the feasibility of targeted optical imaging of ovarian cancer using NIR-830-$Z_{HER2:342}$-IONPs.

2.3 Specifically targeting and optical imaging of HER-2 overexpressing ovarian tumors

Identification of biomarker expression in the tumor using molecular imaging is important for personalized treatment of ovarian cancer patients. To determine whether targeted imaging using NIR-830-$Z_{HER2:342}$–IONPs is able to distinguish between the HER-2 overexpressing and HER-2 low tumors, we used SKOV3 and OVCAR3 human ovarian cancer xenograft models. Optical imaging showed strong signals only in the mice bearing high HER-2 SKOV3 tumors but not in the OVCAR3 tumors (Figure 4A and B).

Signal intensity was 1.73 fold higher in SKOV3 than that of OVCAR3 tumor. Additionally, renal clearance of cleaved NIR dye conjugates is a common feature in our study, which

attributes to the optical signal in the kidney in both non-invasive and *ex vivo* optical imaging. Since the anatomical location of the ovarian tumor in the mice is in the proximity to the kidney, there is a possibility that kidney signal might interfere with tumor imaging. Therefore, we compared the optical signal intensity in the tumor side of the mice with the non-tumor side, where the optical signal was likely from the kidney. Optical signal intensity was 3.3 ± 0.28 fold higher at the side with HER-2 positive SKOV3 tumors than non-tumor side (Figure 4A, n=3). On the other hand, HER-2 low OVCAR3 tumors only showed 1.4 ± 0.15 fold increases in signal intensity in the tumor side compared with the non-tumor side (Figure 4B, n=3). Our results suggested that targeted delivery of NIR-830-$Z_{HER2:342}$–IONPs was more efficient in retaining IONPs in HER-2 positive tumor cells than non-specific nanoparticle delivery into the stroma of the HER-2 low tumors by the enhanced permeability and retention (EPR) effect.

Additionally, systemic delivery of NIR-830-$Z_{HER2:342}$-IONPs was able to target HER-2 positive tumor cells in the ascetic fluids. 24 h after the nanoparticle delivery, ascites collected from the mice bearing SKOV3 tumors had a strong NIR signal (Figure 4C). In contrast, ascites collected from the mice bearing HER-2 low OVCAR3 tumors lacked NIR signal (Figure 4C).

2.4 Importance of active targeting to HER-2 in accumulation of the receptor targeted IONPs in the tumor for sensitive imaging

It is generally accepted that nanoparticles with a size <100 nm can pass through the leaky tumor vasculatures and accumulate in tumor interstitial areas by the EPR effect.[43] It is likely that many tumor cell-targeted nanoparticles utilize the same mechanism entering into the tumor if the cell surface targets are not expressed in tumor endothelial cells. Since tumor endothelial cells do not overexpress HER-2 and murine HER-2 is not recognized by human specific HER-2 affibody $Z_{HER2:342}$, we wanted to determine the role of the EPR effect-mediated intratumoral delivery in HER-2 targeted tumor imaging. Two non-targeted IONPs were used as control IONPs. NIR-830-BSA-IONP has NIR-830-dyes conjugated to BSA molecules and NIR-830-IONP has the dye directly conjugated to the surface polymer coating of the IONP.

To determine the efficiency of active targeting using HER-2 antibody on the delivery and retention of the IONPs in tumors, imaging signals and IONP distributions in the mice bearing SKOV3 tumors following administration of NIR-830-$Z_{HER2:342}$-IONPs, non-targeted NIR-830-BSA-IONPs or NIR-830-IONPs were examined. NIR optical imaging showed significant signal increases in the tumors of the mice that received NIR-830-$Z_{HER2:342}$-IONPs (S/B ratio: 2.8), but not NIR-830-BSA-IONPs (S/B ratio: 1.4) or NIR-830-IONPs (no signal in the tumor) (Figure 5 A, B and C). The mice injected with NIR-830-BSA-IONPs have high body background (Figure 5B), while the mice injected with NIR-830-IONPs showed the highest level of optical signal in the liver (Figure 5C). Similarly, *ex vivo* organ images showed the strongest NIR signal in the tumor of the mice injected with NIR-830-$Z_{HER2:342}$-IONPs but not NIR-830-BSA-IONPs, suggesting specific accumulation of HER-2 targeted NIR-830-$Z_{HER2:342}$-IONPs in the tumor (Figure 5A and B). Moreover, BLI and gross examination of the organs revealed the presence of a thin lay

of disseminated tumor cells on the surface of the spleen, kidney and liver, which was also confirmed by positive optical signals (Figure 5A and B). Prussian blue staining showed selective accumulation of the NIR-830-$Z_{HER2:342}$–IONPs, but not NIR 830-BSA-IONPs, in the tumors (Figure 5A and B). Results of this study support the role of active targeting of HER-2 on tumor cells in the enrichment of the nanoparticles in the tumor mass for sensitive tumor imaging.

2.5 Dual modality imaging of primary and metastatic ovarian tumors using *NIR-830-$Z_{HER2:342}$-IONPs*

NIR dye-labeled IONPs have advantages of tumor imaging using both non-invasive optical and MR imaging, and intraoperative optical imaging. To determine the sensitivity and specificity of NIR-830-$Z_{HER2:342}$-IONPs as MRI contrasts for tumor imaging, MRI was performed prior to and after the administration of the targeted IONPs. SKOV3 tumor bearing mice that received NIR-830-$Z_{HER2:342}$-IONPs showed strong optical signals in the tumor by non-invasive optical imaging (Figure 6A). T_2-weighted MRI revealed a significant MR signal decrease (dark contrast effect) in the tumor 24h after administration of the nanoparticles, indicating accumulation of the IONPs in the tumor. We found that there was an average of 16% signal decrease in the entire tumor (student's T-test: p=0.0004, n=3) (Figure 6A). Non-invasive optical imaging also detected diffused signal in the low peritoneum. Comparison of pre- and post-MR images revealed multiple ~1 mm size round areas that had bright contrasts in the pre-MR image but changed to dark contrasts in the post MR image. Post-mortem gross examination and BLI of the abdominal cavity revealed the presence of metastatic tumor lesions with 1 to 2 mm size on the mesentery of the mice (Figure 6A). Prussian blue staining of tissue sections obtained from disseminated tumors on the mesentery demonstrated the presence of the IONPs in the tumor cells in the metastatic lesion but not in the nearby intestinal mucosa (Figure 6A). However, we also found that it is very challenging to identify numerous (< 1 mm) disseminated tumors on the mesentery when comparing with the pre- and post MR images. As a negative control, MRI scan was conducted in SKOV3 tumor bearing mice injected with NIR-830-BSA-IONPs. There was no MRI contrast change visible in tumor lesions (Figure 6B)

In addition, after systemic delivery of NIR-830-$Z_{HER2:342}$-IONPs, optical imaging detected strong signals both in the primary and metastatic tumors in the gallbladder (Figure 7A). Analysis of the T_2-weighted MR image revealed significant signal decrease in the gallbladder metastases (18.6% of MRI contrast decrease, p=0.02) (Figure 7B). Histological analysis using H&E and Prussian blue staining confirmed the presence of metastatic tumors in the gallbladder and delivery of the IONPs into the tumor (Figure 7C).

3. Discussion

Ovarian cancer is one of the few cancer types that surgically removal of the bulk of the tumors, even when complete surgical resection is impossible, has shown survival benefit in the patients with advanced or recurrent diseases.[44, 45] However, current approaches for the detection of primary tumor and assessment of disseminated tumors do not have sufficient specificity and sensitivity to detect small tumor lesions inside the peritoneal cavity. The development of novel imaging approaches for preoperative detection and staging of the

ovarian cancer and for image-guided surgery, such as receptor targeted dual imaging nanoparticles, should have a great impact on the effective treatment of ovarian cancer.

Optical imaging is a fast, simple, and inexpensive imaging method that can be translated easily into intraoperative imaging in the clinic. Recently, the feasibility of optical imaging of small ovarian cancers using fluorescein isothiocyanate-labeled folic acid probes has been demonstrated in human patients.[46] To improve sensitivity and specificity of *in vivo* tumor imaging, various targeted NIR optical imaging probes have been developed and tested in animal tumor models.[23, 47, 48] Results of our study showed that systemic delivery of NIR-830-$Z_{HER2:342}$-IONPs enabled optical imaging of HER-2 positive ovarian tumors as small as 1 to 2 mm and located > 1 cm deep in the peritoneal cavity. Since each IONP only has ten NIR 830 dye molecules and a total of 4 nmol dye equivalent of IONPs were administrated into each mouse, the fold increases (1.5 to 2.5-folds) of the NIR signal to body background observed in 1 to 2 mm tumors by non-invasive imaging suggested that sufficient amounts of the nanoparticles were delivered into the tumor for sensitive tumor imaging. Although the major limitation for the applications of optical imaging in humans is its low sensitivity in detecting tumors located deep in the body, the sensitivity and detection depth demonstrated in this study should allow intraoperative identification of small tumors seeding on the surface of the omentum and mesentery as well as embedded inside normal tissues or organs in the abdominal cavity by intraoperative optical imaging in human patients. However due to the clearance of NIR-830-dye conjugates through the liver and kidney and non-specific uptake of the nanoparticles by macrophages in the liver and spleen, optical imaging may not be able to sensitively detect metastatic tumor cells on the top or inside the liver, spleen, and kidney within 96 h following the nanoparticle injection.

MRI has high spatial resolution and depth for ovarian cancer imaging in humans. Magnetic IONPs generate strong T_2- and T^*_2-contrast for MRI. It is a class of biocompatible, biodegradable and low toxic nanoparticles. The development of the dual NIR and MR imaging probes should allow detecting ovarian cancer using two imaging modalities that complement each other. Our results demonstrated that T_2-weighted MRI was able to detect orthotopic primary ovarian tumors as well as identify peritoneal metastatic lesions by comparing MRI contrast changes. Therefore, targeted MRI has potential for early detection and accurate assessment of disease stages, which are critical for clinical management of ovarian cancer patients. However, for MRI of tumors in the peritoneal cavity, one problem is that "negative-contrast" in T_2-weighted imaging has a relatively low sensitivity in an abnormal area that has low background signals from surrounding organs, e.g., the liver, spleen, or artifacts from movement of the gut. New MRI imaging methods are under developing in our group using T_1-weighted MRI and ultra short TE imaging sequence to overcome this problem.[49]

To best of our knowledge, current study is the first to apply receptor-targeted dual imaging nanoparticles for the evaluation of nanoparticle targeting efficiency, and the sensitivity and specificity of NIR optical and MR imaging of different stages of ovarian tumors (early or late) in an orthotopic human ovarian cancer xenograft model. Our results demonstrated that HER-2 targeted optical and MR imaging can detect small and large primary tumors,

peritoneal disseminated tumors, and metastatic tumors in the gallbladder and distant organs, such as the lung.

At present, the role of active targeting in intratumoral delivery of nanoparticles is still controversial.[50] This is largely due to the fact that both non-targeted and tumor cell surface molecule-targeted nanoparticles enter into tumor interstitial space through the leaky tumor vasculatures mediated by the EPR effect or passive targeting. [43, 51, 52] However, results of our study clearly showed that active targeting of HER-2 receptor on tumor cells is important for accumulation of sufficient amounts of the targeted IONPs in the tumor for sensitive tumor imaging. It is likely that the binding and internalization of the HER-2 affibody-IONPs in HER-2 expressing tumor cells, as observed in the tumor tissue section by Prussian blue staining, facilitated retention of the IONP in the tumor. Supporting this conclusion, imaging signals and IONPs were not detected in HER-2 positive tumors after delivery of non-targeted IONPs or in HER-2 low expressing tumor following administration of HER-2 targeted IONPs. Without the binding to and being internalized into cells, those small size nanoparticles (18 to 20 nm) could be cleared out from the interstitial space in the tumor in a relatively short time. Unlike big subcutaneous tumors with a high intratumoral interstitial pressure, orthotopic ovarian tumors were highly invasive and readily disseminated into surrounding tissues and the peritoneal cavity. The tumor interstitial pressure may not be very high to generate a strong retention effect on those small nanoparticles as previously reported studies using larger nanoparticles in subcutaneous tumors.

Although HER-2 antibody or antibody has been used to develop optical, PET and single-photon emission computed tomography imaging probes in several other types of HER-2 over-expressing malignant tumors,[25, 53, 54] NIR-830-$Z_{HER2:342}$-IONPs offer several unique characteristics that are well-suited for applications of molecular imaging for the detection of ovarian cancers. First, an affibody has a molecular weight ~ 6 kDa, which is 25 folds smaller than a whole IgG antibody (150 kDa). About 2 to 3 antibodies can be conjugated to a 10 nm core size nanoparticle. However, over 50 of affibody molecules can be conjugated to one nanoparticle. Since the binding affinity of HER-2 affibody is in the picomolar range, excessive amount of high affinity ligands on a nanoparticle may interfere with intratumoral distribution of the nanoparticles. We conjugated 10 affibody molecules to each nanoparticle to achieve adequate binding affinity while facilitating multivalent binding to cellular receptors to enhance receptor-mediated internalization of the nanoparticles. Additionally, selective accumulation of HER-2 targeted nanoparticles in the tumor by the EPR effect and internalization of the nanoparticle into HER-2 over-expressing tumor cells increase tumor signals while having a minimal body background signal that may be generated by a low level of HER-2 expression in normal tissues upon delivery of antibody or antibody fragment-based probes. For example, NIR dye–labeled HER-2 antibody, trastuzumab, has a blood half-life of 5 days following systemic delivery,[55] which can increase the level of body background. However, Kupffer cells in the liver and macrophages in the spleen are only normal cells non-specifically take up nanoparticles due to the leaky sinusoidal clefts. Furthermore, HER-2 affibody-based optical imaging probe has only one C-terminal cysteine for labeling one NIR-830 dye. Each NIR-830-$Z_{HER2:342}$-IONP has multiple HER-2 affibody molecules (~10) that increase the dye concentration in the tumor cells and enhance signal intensity.

Although HER-2 overexpression is well-documented in ovarian cancer patients, HER-2 antibody monotherapy in clinical trials showed a poor therapeutic response. [55–57] Therefore, new therapeutic approaches targeting HER-2 positive ovarian cancers are urgently needed for improving survival of these patients. Currently, we are developing NIR-830-$Z_{HER2:342}$-IONP as a drug carrier for targeted treatment of ovarian cancers. Additionally, malignant ascites are common in ovarian cancer patients. [58] Demonstration of targeted delivery of NIR-830-$Z_{HER2:342}$-IONP into ovarian cancer cells in the ascites shed light on the potential applications on the detection and magnetic enrichment of tumor cells as well as targeted therapy of the ascetic tumor cells.

4. Conclusion

We have developed a new NIR-830 labeled and HER-2 targeted dual imaging modality nanoparticle probe and demonstrated specificity and sensitivity in optical and MR imaging of primary and metastatic ovarian tumors. We further showed that active targeting to tumor cell receptors and binding and internalization of the targeted nanoparticles into tumor cells play important roles in accumulation of the nanoparticles in the tumor and sensitive tumor imaging. This receptor targeted IONP has potential for the development of novel targeted imaging and therapeutic approaches for the detection and effective treatment of ovarian cancer. Additionally, overexpression of HER-2 is also found in several other tumor types, such as breast, pancreatic, gastric and lung cancers. HER-2 targeted dual imaging nanoparticles developed in this study offer an opportunity to develop novel targeted imaging and therapeutic approaches for those cancers.

5. Experimental Section

Tumor Cell lines—High HER-2 expressing SKOV3 human ovarian cancer cell line stably expressing a firefly luciferase gene (SKOV3-luc), provided by Dr. Daniela Matei, at Indiana University Purdue University at Indianapolis (IUPUI, IN), was cultured in McCoy's 5A (Cellgro, Mediatech Inc) supplemented with 10% fetal bovine serum (Hyclone, Thermo scientific) and 1% penicillin and streptomycin (Hyclone). The low HER-2 expressing OVCAR3 human ovarian cancer cell line was from Dr. Neil Gidell at Emory University. Cells were cultured in RPMI-1640 (Cellgro, Mediatech Inc.) supplemented with 10% fetal bovine serum and 1% penicillin and streptomycin. The cultured cells were maintained at 37°C and 5% CO_2 in a tissue culture incubator. The levels of HER-2 expression in above cell lines were determined by Western blot and immunofluorescence labeling.

Western Blot—Cells were lysed in a lysis buffer containing protease inhibitor cocktail (Sigma–Aldrich). Cell lysates were sonicated briefly and subjected to centrifugation at 14,000 rpm for 15 min at 4°C. Equal amounts of protein (100 μg) from cell lysates were separated by 7% SDS-PAGE and electroblotted onto polyvinylidene difluoride membranes (Bio-Rad laboratories). After blocking, the membranes were probed with the primary antibody for overnight at 4°C with gentle rocking. Antibodies used are epidermal growth factor receptor-2 (HER-2, 1:1,000 dilutions; Calbiochem,) and β-actin (Sigma–Aldrich) at 1:10,000. Appropriate secondary antibodies were used at 1:5,000 dilutions (Santa Cruz Inc,) After incubation with specific horseradish peroxidase -conjugated secondary antibody,

HER-2 protein was visualized using the enhanced chemiluminescence detection system (GE Healthcare) and autoradiography.

Immunofluorescence—Cells were placed on glass chamber slides (Nalge Nunc International) and allowed to adhere. After fixation in 4% paraformaldehyde in PBS, cells were permeabilized in 0.2% Triton X-100 in PBS for 15 min, and then blocked with 3% goat serum in PBS for 1 h. Cells were incubated with the primary antibody diluted in blocking buffer at room temperature for 2 h (HER-2 antibody cat # 2242, 1:100 dilution; Cell Signaling) followed by a 30 min incubation with Alexa Fluor-488 labeled anti-rabbit secondary antibody (Cat # A11034,1:1,000, Invitrogen). Cell nuclei were visualized by Hoechst 33342 staining. The slides were examined under a fluorescence microscope (Zeiss Axioplan).

Magnetic IONPs were prepared using iron oxide powder as the iron precursor, oleic acid as the ligand and octadecene as the solvent.[59] The core size and hydrodynamic size of the nanoparticles were measured using transmission electron microscopy (TEM), and light scattering scan, respectively. The particles were coated with amphiphilic polymers using our established protocols.[33, 38, 60, 61] In brief, IONPs and polymaleic anhydride-alt-1-octadecene polymer were mixed in chloroform at a 1:10 molar ratio for 1 h. Water was then added to the mixture at a 1:1 volume ratio, and the resulting heterogeneous mixture was subjected to rotary evaporation, which yielded a clear aqueous solution of IONPs. The particles were purified by high-speed centrifugation, and then resuspended in Borate buffer (pH 8.5, 50 mM). The concentration of the nanoparticles was determined by X-ray fluorescent spectra. The optical density of 0.1 mg/mL IONPs at 500 nm is 1.

Production of NIR-830-$Z_{HER2:342}$-IONPs—HER-2 affibody ($Z_{HER2:342}$-Cys) was produced from a bacterial expressing system using an established protocol.[21] The gene sequence for $Z_{HER2:342}$ can be obtained from the following reference [22] $Z_{HER2:342}$-Cys was subjected to reduction with 5 mM 2-carboxyethyl phosphine hydrochloride (TCEP) and then labeled with NIR 830-maleimide dye, synthesized from IR-783 dye (Sigma-Aldrich) in our group, through forming a thio-ester bond between the thio group of a unique cysteine at the C-terminus of HER-2 affibody and the maleimide group of NIR-830 dye (Figure 1A and Supporting Information S1). Ten NIR-830-HER-2 affibody molecules were then conjugated to each amphiphilic polymer-coated IONP (10 nm core size) via an amide bond mediated by ethyl-3-dimethyl amino propyl-carbodiimide and sulfo-N-hydroxy succinimide (Sigma) (Figures 1A and Supporting Information S1). The NIR-830-$Z_{HER2:342}$-IONP conjugates were purified using Nanosep 100 K column (Pall Corporation) and resuspended in Borate buffer, pH 8.6, and stored at 4 °C. Similarly, BSA was labeled with NIR dye followed by IONP conjugation. The final concentration of iron (mg/ml) in the conjugate was determined by using absorbance at 500 nm x dilution factor/4.3. Based on the Bradford protein assay, we determined that the average number of 10 affibody molecules were conjugated to each IONP. Since each affibody only labeled with one NIR-830 dye molecule, 1 mg of iron equivalent IONPs or 907 pmol of IONPs only have 9 nmol of NIR 830 dye molecules conjugated to the HER-2 affibody. For *in vivo* imaging, 400 pmol of NIR-830-$Z_{HER2:342}$-

IONPs (total amount of IONPs) were used for each mouse, which only contain 4 nmol or 3.8 μg of NIR-830 dye molecules.

Average hydrodynamic sizes and zeta potentials of the nanoparticles were measured using a dynamic light scattering (DLS) instrument (Zetasizer Nano-ZS S-90, Malvern Instruments).

Specificity of NIR-830-$Z_{HER2:342}$-IONPs—SKOV3 (HER-2 high) and OVCAR3 (HER-2 low) cells cultured in 24-well plates were incubated with 100 nM of iron equivalent IONP concentration of NIR-830-$Z_{HER2:342}$-IONPs and control non-conjugated IONPs at 37°C for 4 h. Cells were fixed with 4% formaldehyde followed by Prussian blue staining using a 1:1 mixture of 10% potassium ferrocyanide, trihydrate (MP Biomedical) and 10% hydrochloric acid at 37°C for 30 min. The presence of cellular uptake of IONPs was examined by an inverted microscope.

Orthotropic Human Ovarian Cancer Xenograft Model—The orthotopic human ovarian cancer xenograft models were established by injecting 5×10^4 SKOV3-luc or OVCAR3 cancer cells in 15 μl of PBS into the ovary bursa of 6–8 week old female athymic nude mice by surgery (Harlan laboratories) (Figure S2). All mouse surgical and imaging procedures were approved by the Institutional Animal Care and Use Committee of Emory University. Growth of SKOV3-luc tumors was monitored and quantified weekly using a bioluminescence imaging (BLI) system (Caliper Life Sciences). The growth of OVCAR3 tumor xenografts was confirmed after sacrificing the mice. SKOV3-luc tumor bearing mice were administered intraperitoneally with 30 mg/kg of luciferase substrate (D-luciferin) 10 minutes prior to the imaging. For quantification of BLI, Regions of Interest (ROIs) in the tumor area as well as body background were selected. Then integrated flux of photons (photons/sec) within each region was calculated using the software provided by the Caliper Life Sciences.

***In Vivo* Tumor Imaging—**Mice were subjected to NIR optical and MR imaging 1 to 6 weeks after implanting tumor cells into the ovary bursa. 400 pmol of NIR-830-$Z_{HER2:342}$-IONPs were injected via the tail vein. NIR optical imaging was conducted using the Kodak *In vivo* FX imaging system (Carestream Health Inc). For biodistribution studies, tumor-bearing mice were sacrificed and tumors and normal organs were removed for *ex vivo* optical imaging. Ascites in the peritoneal cavity of the tumor-bearing mice were collected for optical imaging. All optical images were captured using 800 nm excitation and 850 nm emission filter set with 180 sec exposure time and a Gamma value of 0.2. Optical Images were analyzed using the software provided by the imaging system. ROIs were selected for measuring the mean fluorescence intensity (MFI) of tumors and corresponding body background. Signal to body background (S/B) ratio was calculated from the MFI of the tumor area divided by of the body background area. Data shown in Results were the mean S/B ratio ± standard derivation from three to nine mice.

MRI was performed on mice using a 3 T (Tesla) MRI scanner (Siemens Medical System) with a customized rodent coil. T_2-weighted fast spin echo (FSE) imaging sequence with TR of 5000 ms, TE of 28 ms, field of view of 40 × 70 mm, and slice thickness of 1 mm were used to acquire pre- and post-contrast MR images. MRI Contrast change in tumor following

administration of the targeted nanoparticles was quantitatively analyzed using the ROI method and ImageJ software (National Institutes of Health). Averaged signal intensities of the ROI were obtained from tumor and control muscle area. MRI contrast intensity in the tumor was normalized with the muscle contrast for each MR image as the intensity of tumor contrast/muscle contrast. MRI contrast changes were calculated as post-MRI contrast intensity/pre-MRI contrast intensity × 100. The percentage of mean MR contrast change was calculated from three to four MR image slices.

Histology

Following optical/MR imaging, mice were sacrificed and tumors and organs were collected for histological analysis. Morphology of the tissues was evaluated by haematoxylin and eosin (H&E) staining of 5 μm paraffin tissue sections. Prussian blue staining was performed for the detection of iron in the tissue sections. The images were acquired at 100 or 200X magnifications by Zeiss Axioplan 2 upright microscope.

Statistical analyses

All data were presented as mean ± standard deviation from at least triplicate samples. Statistical analysis was conducted using Student's *t*-test or paired *t*-test. Statistically significant difference was defined as values of $p < 0.05$.

Supplementary Material

Refer to Web version on PubMed Central for supplementary material.

Acknowledgments

We thank Drs. Daniela Matei and Neil Sidell for providing SKOV3-Luc cell and OVCAR3 cell lines. This research project was supported by the following NIH/NCI grants, R01CA132722 (Yang) and U01CA151810 (Yang and Mao), and the Nancy Panoz Endowed Chair Funds (Yang).

References

1. Naora H, Montell DJ. Nat Rev Cancer. 2005; 5:355. [PubMed: 15864277]
2. Moss C, Kaye SB. Eur J Cancer. 2002; 38:1701. [PubMed: 12175685]
3. De Souza R, Zahedi P, Moriyama EH, Allen CJ, Wilson BC, Piquette-Miller M. Mol Cancer Ther. 2010; 9:1820. [PubMed: 20530719]
4. Bast RC Jr, Hennessy B, Mills GB. Nat Rev Cancer. 2009; 9:415. [PubMed: 19461667]
5. Cannistra SA. N Engl J Med. 2004; 351:2519. [PubMed: 15590954]
6. Agarwal R, Kaye SB. Nat Rev Cancer. 2003; 3:502. [PubMed: 12835670]
7. Vaughan S, Coward JI, Bast RC Jr, Berchuck A, Berek JS, Brenton JD, Coukos G, Crum CC, Drapkin R, Etemadmoghadam D, Friedlander M, Gabra H, Kaye SB, Lord CJ, Lengyel E, Levine DA, McNeish IA, Menon U, Mills GB, Nephew KP, Oza AM, Sood AK, Stronach EA, Walczak H, Bowtell DD, Balkwill FR. Nat Rev Cancer. 2011; 11:719. [PubMed: 21941283]
8. Kyriazi S, Kaye SB, deSouza NM. Nat Rev Clin Oncol. 2010; 7:381. [PubMed: 20386559]
9. Nahta R, Yu D, Hung MC, Hortobagyi GN, Esteva FJ. Nat Clin Pract Oncol. 2006; 3:269. [PubMed: 16683005]
10. Guzzo F, Bellone S, Buza N, Hui P, Cantuaria L, Varughese J, Cocco E, Betti M, Todeschini P, Gasparrini S, Schwartz PE, Rutherford TJ, Angioli R, Pecorelli S, Santin AD. Int J Gynecol Pathol. 2012; 31:211. [PubMed: 22498937]

11. Chavez-Blanco A, Perez-Sanchez V, Gonzalez-Fierro A, Vela-Chavez T, Candelaria M, Cetina L, Vidal S, Duenas-Gonzalez A. BMC Cancer. 2004; 4:59. [PubMed: 15341668]
12. Jaeone J, Urmacher C, Thaler HT, Friedlander-Klar H, Cordon-Cardo C, Meyer HJ. J Cancer Res Clin Oncol. 1992; 118:474. [PubMed: 1352299]
13. Ochs AM, Wong L, Kabani V, Neerukonda S, Gorske J, Rao A, Riggs M, Ward H, Keville L. Clin Colorectal Cancer. 2004; 4:262. [PubMed: 15555209]
14. Livasy CA, Reading FC, Moore DT, Boggess JF, Lininger RA. Gynecol Oncol. 2006; 100:101. [PubMed: 16157366]
15. Sauter ER, Keller SM, Ernst S, Goldberg M. Cancer Lett. 1993; 75:41. [PubMed: 7904538]
16. Kern JA, Schwartz DA, Nordberg JE, Weiner DB, Greene MI, Torney L, Robinson RA. Cancer Res. 1990; 50:5184. [PubMed: 1974168]
17. Lei S, Appert HE, Nakata B, Domenico DR, Kim K, Howard JM. Int J Pancreatol. 1995; 17:15. [PubMed: 8568330]
18. Meden H, Marx D, Roegglen T, Schauer A, Kuhn W. Int J Gynecol Pathol. 1998; 17:61. [PubMed: 9475194]
19. Cirstoiu-Hapca A, Buchegger F, Lange N, Bossy L, Gurny R, Delie F. J Control Release. 2010; 144:324. [PubMed: 20219607]
20. Lee JH, Huh YM, Jun YW, Seo JW, Jang JT, Song HT, Kim S, Cho EJ, Yoon HG, Suh JS, Cheon J. Nat Med. 2007; 13:95. [PubMed: 17187073]
21. Zielinski R, Hassan M, Lyakhov I, Needle D, Chernomordik V, Garcia-Glaessner A, Ardeshirpour Y, Capala J, Gandjbakhche A. PLoS One. 2012; 7:e41016. [PubMed: 22911732]
22. Orlova A, Magnusson M, Eriksson TL, Nilsson M, Larsson B, Hoiden-Guthenberg I, Widstrom C, Carlsson J, Tolmachev V, Stahl S, Nilsson FY. Cancer Res. 2006; 66:4339. [PubMed: 16618759]
23. Lee SB, Hassan M, Fisher R, Chertov O, Chernomordik V, Kramer-Marek G, Gandjbakhche A, Capala J. Clin Cancer Res. 2008; 14:3840. [PubMed: 18559604]
24. Kramer-Marek G, Gijsen M, Kiesewetter DO, Bennett R, Roxanis I, Zielinski R, Kong A, Capala J. J Nucl Med. 2012; 53:629. [PubMed: 22410461]
25. Baum RP, Prasad V, Muller D, Schuchardt C, Orlova A, Wennborg A, Tolmachev V, Feldwisch J. J Nucl Med. 2010; 51:892. [PubMed: 20484419]
26. Gao J, Chen K, Miao Z, Ren G, Chen X, Gambhir SS, Cheng Z. Biomaterials. 2011; 32:2141. [PubMed: 21147502]
27. Alexis F, Basto P, Levy-Nissenbaum E, Radovic-Moreno AF, Zhang L, Pridgen E, Wang AZ, Marein SL, Westerhof K, Molnar LK, Farokhzad OC. Chem Med Chem. 2008; 3:1839. [PubMed: 19012296]
28. Kinoshita M, Yoshioka Y, Okita Y, Hashimoto N, Yoshimine T. Contrast Media Mol Imaging. 2010; 5:18. [PubMed: 20140973]
29. Schultz JF, Bell JD, Goldstein RM, Kuhn JA, McCarty TM. Ann Surg Oncol. 1999; 6:691. [PubMed: 10560816]
30. Harisinghani MG, Barentsz J, Hahn PF, Deserno WM, Tabatabaei S, van de Kaa CH, de la Rosette J, Weissleder R. N Engl J Med. 2003; 348:2491. [PubMed: 12815134]
31. Weissleder R, Ntziachristos V. Nat Med. 2003; 9:123. [PubMed: 12514725]
32. Kircher MF, Mahmood U, King RS, Weissleder R, Josephson L. Cancer Res. 2003; 63:8122. [PubMed: 14678964]
33. Yang L, Peng XH, Wang YA, Wang X, Cao Z, Ni C, Karna P, Zhang X, Wood WC, Gao X, Nie S, Mao H. Clin Cancer Res. 2009; 15:4722. [PubMed: 19584158]
34. Medarova Z, Pham W, Kim Y, Dai G, Moore A. Int J Cancer. 2006; 118:2796. [PubMed: 16385568]
35. Montet X, Montet-Abou K, Reynolds F, Weissleder R, Josephson L. Neoplasia. 2006; 8:214. [PubMed: 16611415]
36. Tomanek B, Iqbal U, Blasiak B, Abulrob A, Albaghdadi H, Matyas JR, Ponjevic D, Sutherland GR. Neuro Oncol. 2012; 14:53. [PubMed: 22013169]
37. Kircher MF, Weissleder R, Josephson L. Bioconjug Chem. 2004; 15:242. [PubMed: 15025519]

38. Yang L, Mao H, Cao Z, Wang YA, Peng X, Wang X, Sajja HK, Wang L, Duan H, Ni C, Staley CA, Wood WC, Gao X, Nie S. Gastroenterology. 2009; 136:1514. [PubMed: 19208341]
39. Key J, Cooper C, Kim AY, Dhawan D, Knapp DW, Kim K, Park JH, Choi K, Kwon IC, Park K, Leary JF. J Control Release. 2012; 163:249. [PubMed: 22902594]
40. Xie J, Chen K, Huang J, Lee S, Wang J, Gao J, Li X, Chen X. Biomaterials. 2010; 31:3016. [PubMed: 20092887]
41. Lee CL, Qian WP, Wang L, Wang YA, Staley CA, Satpathy M, Nie S, Mao H, Yang L. ACS Nano. 2013; 7:2078. [PubMed: 23402593]
42. Kerr VE, Cadman E. Cancer. 1985; 56:1209. [PubMed: 4016709]
43. Terrault SD, Walkey C, Jennings T, Fischer HC, Chan WC. Nano Lett. 2009; 9:1909. [PubMed: 19344179]
44. Bristow RE, Tomacruz RS, Armstrong DK, Trimble EL, Montz FJ. J Clin Oncol. 2002; 20:1248. [PubMed: 11870167]
45. Rose PG, Nerenstone S, Brady MF, Clarke-Pearson D, Olt G, Rubin SC, Moore DH, Small JM. N Engl J Med. 2004; 351:2489. [PubMed: 15590951]
46. van Dam GM, Themelis G, Crane LM, Harlaar NJ, Pleijhuis RG, Kelder W, Sarantopoulos A, de Jong JS, Arts HJ, van der Zee AG, Bart J, Low PS, Ntziachristos V. Nat Med. 2011; 17:1315. [PubMed: 21926976]
47. Yang X, Shi C, Tong R, Qian W, Zhau HE, Wang R, Zhu G, Cheng J, Yang VW, Cheng T, Henary M, Strekowski L, Chung LW. Clin Cancer Res. 2010; 16:2833. [PubMed: 20410058]
48. Hilderbrand SA, Weissleder R. Curr Opin Chem Biol. 2010; 14:71. [PubMed: 19879798]
49. Zhang L, Zhong X, Wang L, Chen H, Wang YA, Yeh J, Yang L, Mao H. J Magn Reson Imaging. 2011; 33:194. [PubMed: 21182139]
50. Pirollo KF, Chang EH. Trends Biotechnol. 2008; 26:552. [PubMed: 18722682]
51. Prabhakar U, Maeda H, Jain RK, Sevick-Muraca EM, Zamboni W, Farokhzad OC, Barry ST, Gabizon A, Grodzinski P, Blakey DC. Cancer Res. 2013; 73:2412. [PubMed: 23423979]
52. Jain RK, Stylianopoulos T. Nat Rev Clin Oncol. 2010; 7:653. [PubMed: 20838415]
53. Orlova A, Tolmachev V, Pehrson R, Lindborg M, Tran T, Sandström M, Nilsson FY, Wennborg A, Abrahmsen L, Feldwisch J. Cancer Res. 2007; 67:2178. [PubMed: 17332348]
54. Orlova A, Wallberg H, Stone-Elander S, Tolmachev V. J Nucl Med. 2009; 50:417. [PubMed: 19223403]
55. Bookman MA, Darcy KM, Clarke-Pearson D, Boothby RA, Horowitz IR. J Clin Oncol. 2003; 21:283. [PubMed: 12525520]
56. Gordon MS, Matei D, Aghajanian C, Matulonis UA, Brewer M, Fleming GF, Hainsworth JD, Garcia AA, Pegram MD, Schilder RJ, Cohn DE, Roman L, Deyrup MK, Ng K, Lyons B, Allison DE, Eberhard DA, Pham TQ, Dere RC, Karlan BY. J Clin Oncol. 2006; 24:4324. [PubMed: 16896006]
57. Tuefferd M, Couturier J, Penault-Llorca F, Vincent-Salomon A, Broet P, Guastalla JP, Allouache D, Combe M, Weber B, Pujade-Lauraine E, Camilleri-Broet S. PLoS One. 2007; 2:e1138. [PubMed: 17987122]
58. Scarberry KE, Dickerson EB, Zhang ZJ, Benigno BB, McDonald JF. Nanomedicine. 2010; 6:399. [PubMed: 19969103]
59. Yu WW, Falkner JC, Yavuz CT, Colvin VL. Chem Commun (Camb). 2004:2306. [PubMed: 15489993]
60. Chen K, Xie J, Xu H, Behera D, Michalski MH, Biswal S, Wang A, Chen X. Biomaterials. 2009; 30:6912. [PubMed: 19773081]
61. Duan MKH, Wang X, Wang YA, Nie S, Mao H. J Phys Chem. 2008:348

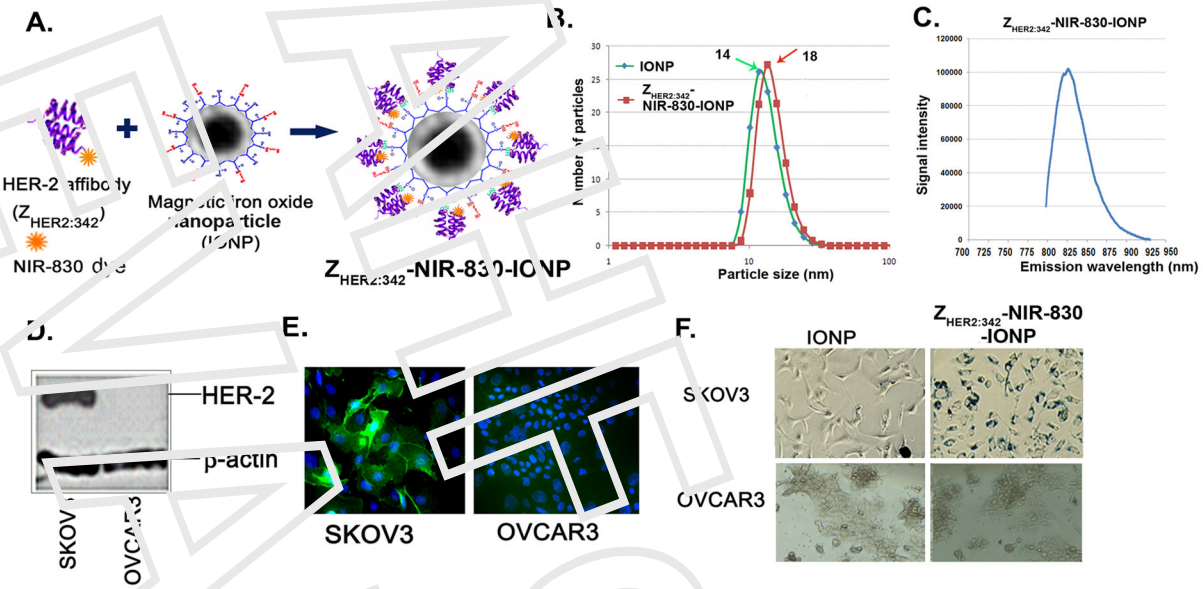

Figure 1. Characterization of NIR-830-$Z_{HER2:342}$-IONP

(A) Illustration of structure of a NIR-830-$Z_{HER2:342}$-conjugated IONP. (B) Hydrodynamic size of non-conjugated IONPs and NIR-830-$Z_{HER2:342}$-IONPs determined by DLS. (C) NIR-830-$Z_{HER2:342}$-IONPs has a peak emission wavelength between 825–830nm. (D and E) The levels of HER-2 expression in SKOV3 and OVCAR3 cell lines determined by Western blot and immunofluorescence labeling. (F) Visualization of internalized IONPs by microscopy after Prussian blue staining

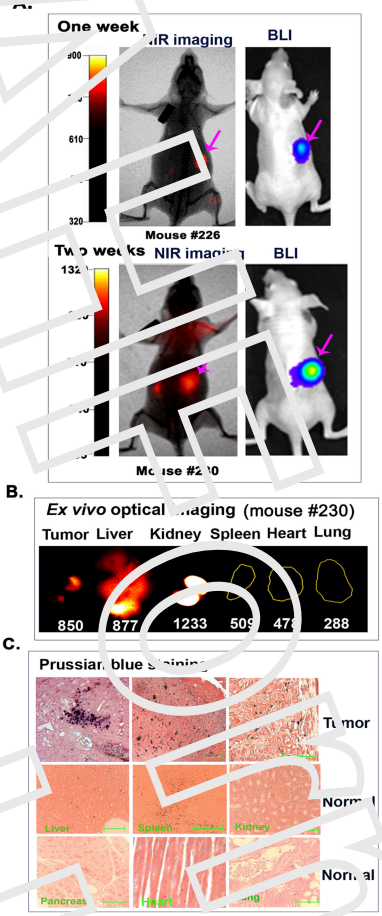

Figure 2. Detection of the early stage ovarian cancer by optical imaging

(A) NIR optical imaging of representative mice at one (upper) or two (lower) weeks after SKOV3 cell implantation and 24 h following tail vein delivery of NIR-830-$Z_{HER2:342}$–IONPs. Strong optical signals were detected in the tumors that were identified by BLI. Three mice were examined at each time point. (B) *Ex vivo* NIR imaging showing optical signals in tumor, liver and kidney but not in the spleen, heart and lung. (C) Prussian blue staining showed iron positive cells in various tumor areas (upper panel). Low to intermediate levels of iron positive cells were only found the liver and spleen but not in the kidney, pancreas, heart, and lung. Scale bars represent 50 μM.

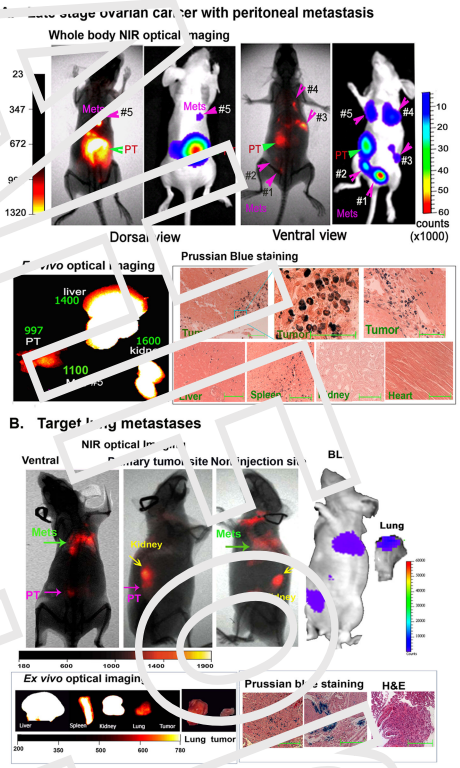

Figure 3 Detection of the late stage ovarian cancer by non-invasive optical imaging

(A) NIR optical imaging of a representative mouse bearing primary and metastatic ovarian tumors at 24 h following NIR-830-$Z_{HER2:342}$-IONP administration. Optical imaging detected a primary and five metastatic tumors that were identified by BLI. Green arrow: primary tumor. Pink arrows: metastases. Similar results were found in 9 mice. PT: primary tumor. Mets: metastases. *Ex vivo* NIR imaging: numbers shown are the mean fluorescence intensity of tumors or normal organs. Prussian blue staining showed the iron containing cells in the peripheral and central tumor areas. High magnification microscopic image (200×) showed internalization of the targeted IONPs in tumor cells. Blue square and lines indicated the tissue image from the same area. **(B)** Strong NIR signal was detected in a mouse with lung metastases (green arrows). BLI confirmed the presence of the tumor cells in the lung. *Ex vivo* optical imaging showing strong NIR signals in the liver, kidney, spleen, tumor and lung. Bright field images of the lung and tumor are included. Histological analysis confirmed the presence of lung metastasis by H&E staining and iron positive cells by Prussian blue staining (10X magnifications). Scale bars represent 50 μM.

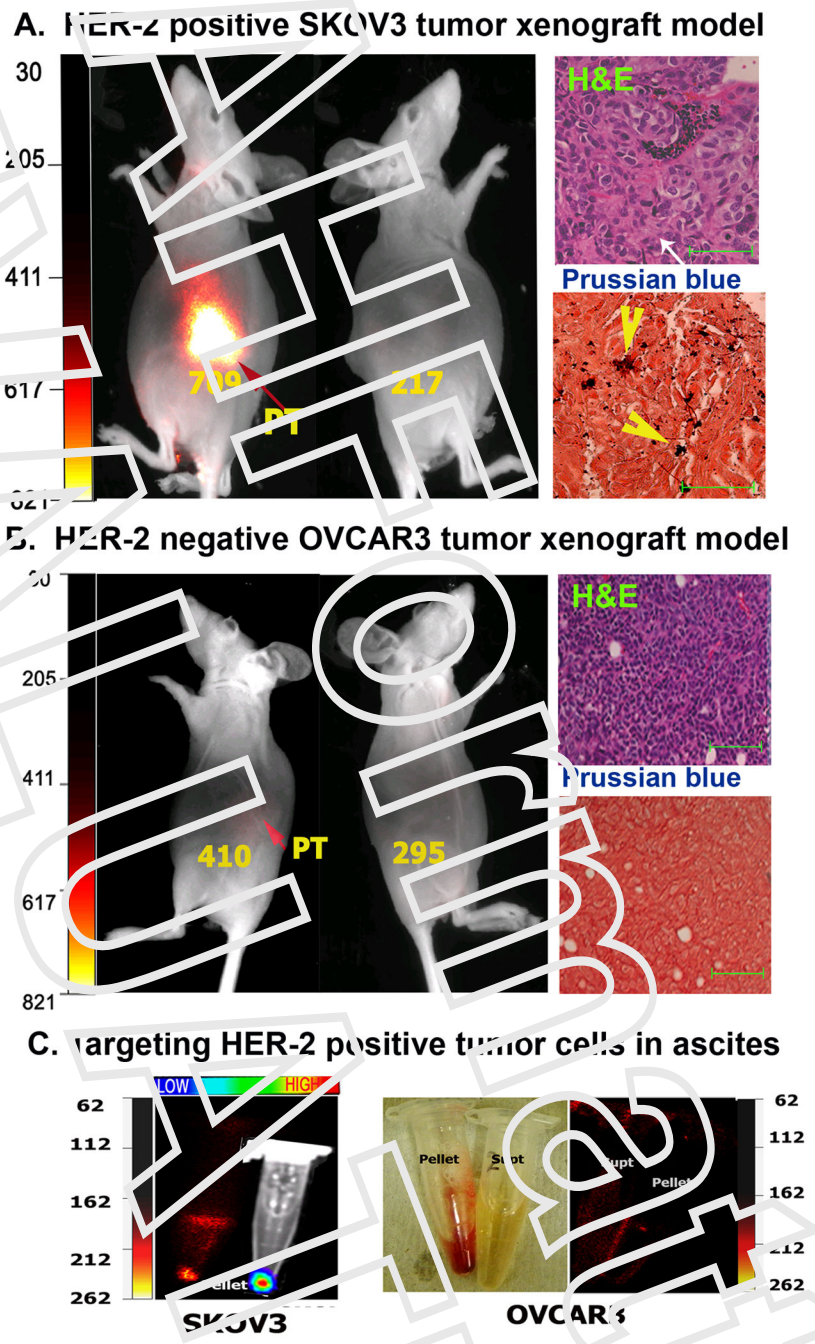

Figure 4. Specific *in vivo* optical imaging of HER-2 positive ovarian tumors using NIR-830-$Z_{HER2:342}$-IONP

A. Mice bearing HER-2 positive SKOV3 tumors have a strong signal in the tumor 24h after NIR-830-$Z_{HER2:342}$-IONP injection. Mean fluorescence intensities of the tumor area and the non-tumor side were shown in the figure. Prussian blue staining confirmed the iron positive tumor cells (Magnification 100X). Scale bars represent 50 μM. **B.** Mice bearing low HER-2 expressing OVCAR3 tumors displayed weak signals in the tumor area following NIR-830-$Z_{HER2:342}$-IONP administration. The IONP positive cells were not found in the tumor sections after Prussian blue staining. **C.** Ascites collected from SKOV3 tumor bearing

mouse, but not from OVCAR3 tumor bearing mouse, showed NIR signal in the cell pellet. BLI confirmed the presence of SKOV3 cells in the pellet. A bright field image of a cell pellet collected from an OVCAR3 tumor bearing mouse was shown.

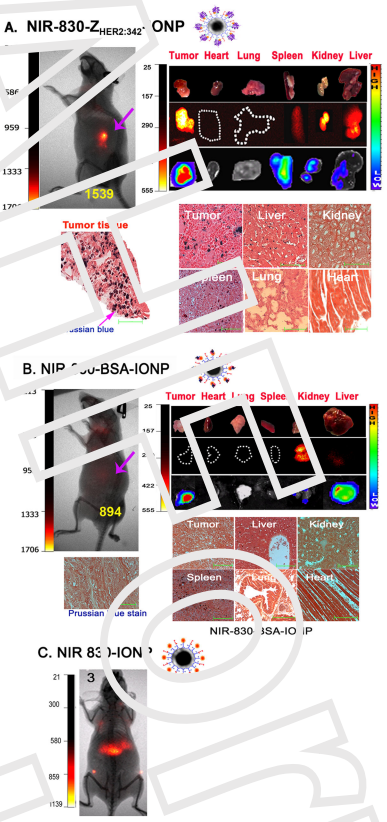

Figure 5. Determination of *in vivo* target specificity of NIR-830-$Z_{HER2:342}$-IONP

SKOV3 tumor bearing mice received 400 pmol of NIR-830-$Z_{HER2:342}$-IONPs, non-specific NIR-830-BSA-IONPs, or NIR-830-IONPs. **A.** A representative mouse received NIR-830-$Z_{HER2:342}$-IONP (n=15). Pink arrow: primary tumor. *Ex vivo* organ imaging: Upper: picture of tumor and organs; Middle: optical images showed signals in the tumor and the spleen, kidney and liver. Bottom: Bioluminescence images confirm the presence of ovarian cancer cells on the surface of the organs. Prussian blue staining demonstrated IONP positive cells in the tumors, liver and spleen. Scale bars represent 50 μM. **B.** A representative mouse received NIR-830-BSA-IONP (n=4). Optical signals and Prussian blue positive cells were not detected in the tumor. **C.** A mouse received NIR-830-IONP (n=3). Only the liver showed optical signal. Numbers in the optical images are the mean ROI intensities of tumor areas.

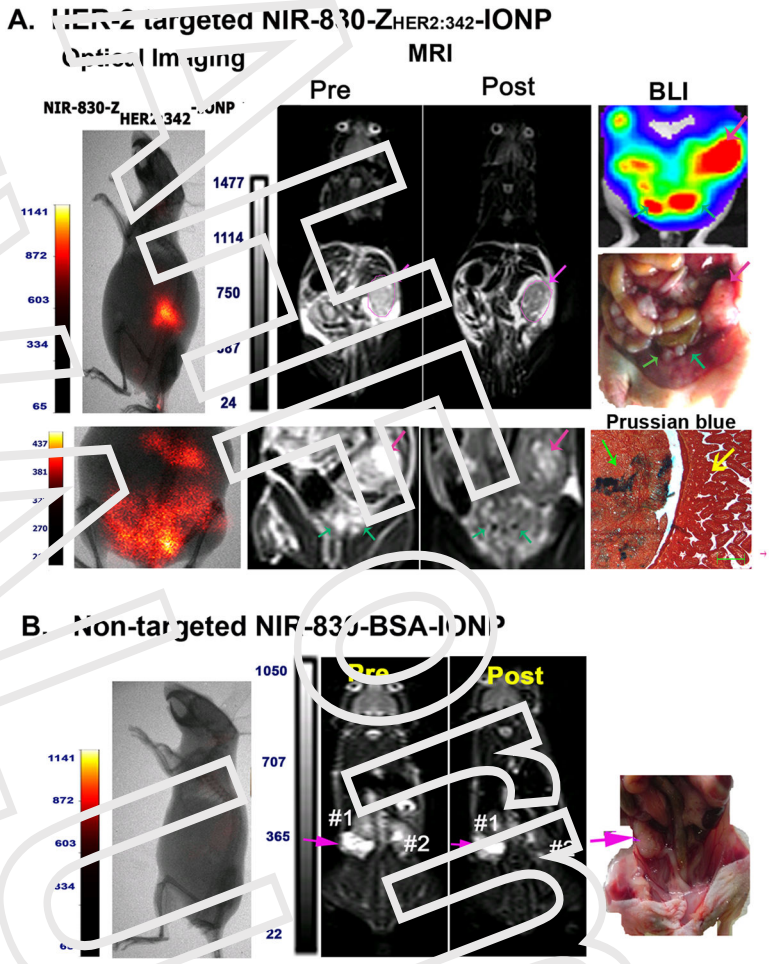

Figure 6. Dual modality imaging of SKOV3 tumor bearing mice

A. Optical imaging revealed strong signals in the primary tumor and peritoneal metastases in the tumor bearing mice following NIR-830-$Z_{HER2:342}$-IONP administration. T_2-weighted MRI also showed marked signal decrease (16%) in a large primary tumor (pink arrow) and small peritoneal metastases (Green arrow), which were identifiable by BLI and gross examination after sacrificing the mouse. Prussian blue staining confirmed the delivery of the targeted IONPs into primary tumor and mesentery metastases. Scale bars represent 10 μM. **B.** MRI of SKOV3 tumor bearing mice after NIR-830-BSA-IONP injection. There was no contrast change in pre- and post-MR images of the tumor.

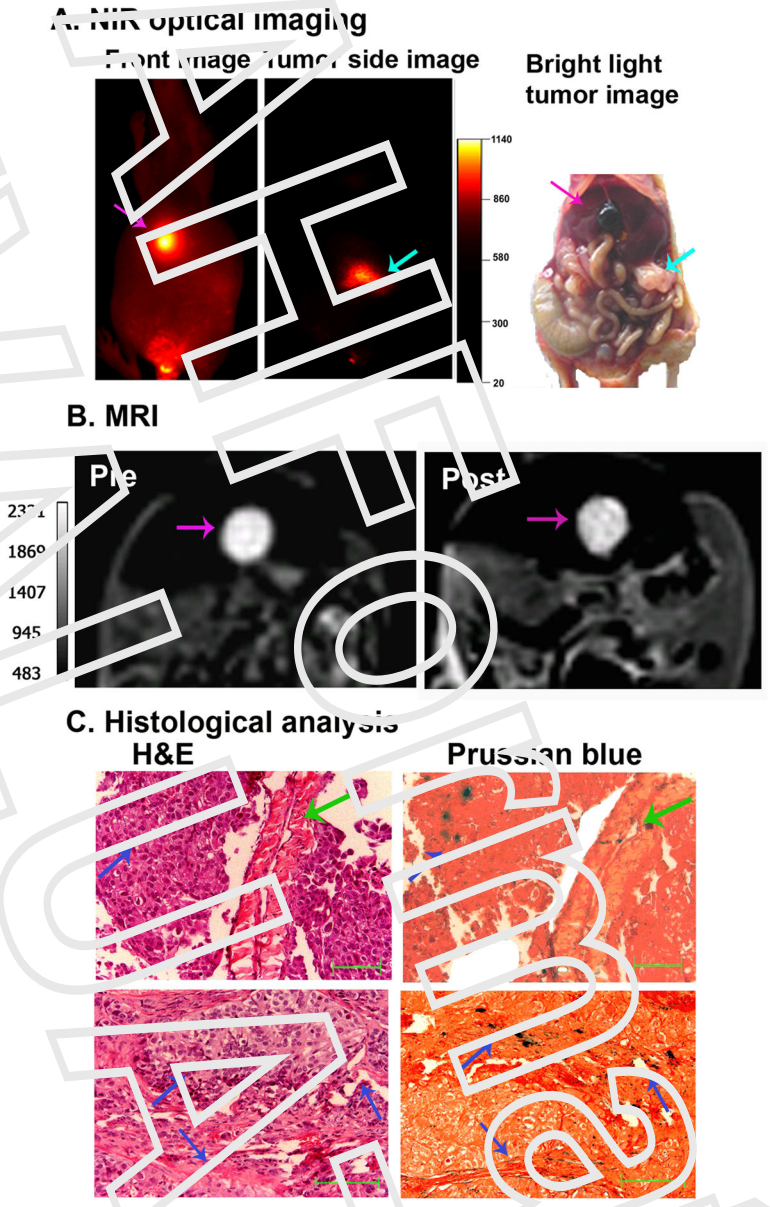

Figure 7. Dual modality imaging of a gallbladder metastatic tumor following systemic delivery of NIR-830-$Z_{HER2:342}$-IONP

A. NIR optical imaging of a representative SKOV3 tumor bearing mouse injected with NIR-830-$Z_{HER2:342}$-IONP. Left panel showing a strong NIR fluorescence signal in the gallbladder metastasis; Middle panel showing NIR signal in the primary tumor at the injection site; Right panel showing corresponding camera image of the primary tumor and enlarged gallbladder in the mouse. Pink arrow: gallbladder metastases, Light blue arrow: primary tumor. **B.** MR images of the mouse showing T_2 contrast change in the gallbladder (Pre and Post NIR-830-$Z_{HER2:342}$-IONP delivery). **C.** Histological analysis of gallbladder tissue by H&E staining and Prussian blue stain. The presence of metastatic tumors and the IONP-positive tumor cells in the gallbladder was observed in the tissue sections. Green

arrow: Smooth muscle wall of the gallbladder; Dark blue arrow: metastatic tumors. Scale bars represent 50 μM.